Deep-Sea Research I 67 (2012) 85–97

Contents lists available at SciVerse ScienceDirect

Deep-Sea Research I

journal homepage: www.elsevier.com/locate/dsri

An evaluation of tracer fields and anthropogenic carbon in the equatorial and the tropical North Atlantic

A. Schneider [a,*], T. Tanhua [a], A. Körtzinger [a], D.W.R. Wallace [b]

[a] Helmholtz-Zentrum für Ozeanforschung (GEOMAR), Marine Biogeochemie, Kiel, Germany
[b] Department of Oceanography, Dalhousie University, Halifax, Nova Scotia, Canada

ARTICLE INFO

Article history:
Received 10 November 2011
Received in revised form
28 April 2012
Accepted 14 May 2012
Available online 7 June 2012

Keywords:
Anthropogenic carbon
Tracer
TTD
Tropical Atlantic
Mean age

ABSTRACT

The transit time distribution method was applied to dichlorodifluoromethane and sulfur hexafluoride measurements from four cruises to the tropical North Atlantic between 2006 and 2009 in order to estimate anthropogenic carbon (C_{ant}) concentrations. By assuming an Inverse Gaussian distribution of the transit time distribution the best fit to the data was achieved with the ratio of mean age to width equals 1. Significant differences in the mean age and C_{ant} concentrations between the equatorial belt (5°S–5°N) and the Guinea dome area (5°–15°N) was found. Mean ages are higher and C_{ant} concentrations are lower in the Guinea dome area than at same depths, or densities, in the equatorial belt. The mean column inventories in the upper 1200 m are higher by about 3 mol m^{-2} in the equatorial belt compared to the Guinea dome area. The mean column inventory of C_{ant}, for the whole water column, in the tropical Atlantic is 32.2 mol m^{-2} (error range: 30.6–45.2 mol m^{-2}), which is significantly lower than the previous estimates. The total C_{ant} inventory in the eastern tropical Atlantic is 2.5 Pg (error range: 2.3–3.5 Pg) for an area of 6×10^6 km^2, comprising the Guinea dome region and the equatorial belt. The equatorial belt has 40% higher storage of C_{ant} compared to the Guinea dome area which reflects the occurrence of relatively young deep waters at the equator, being high in anthropogenic carbon. Our tracer based C_{ant} estimates were compared to C_{ant} concentrations calculated with the TrOCA method applied to measurements conducted in 1999. The TrOCA based estimates are significantly higher than our tracer based C_{ant} estimates. Comparison between tracer measurements in 1999 and the 2006–2009 time-frame revealed possible speed-up of ventilation in the upper water column, increasing the C_{ant} concentration in this depth range at a faster rate and a C_{ant} increase of 12.1 μmol kg^{-1} in the tropical surface water was found.

1. Introduction

The rate of atmospheric carbon dioxide (CO_2) increase of more than 100 ppm since the late 18th century is exceptional in Earth's history and has been clearly ascribed to anthropogenic emissions. About 50% of the anthropogenic CO_2 (C_{ant}) has been taken up by the ocean and the biosphere (Denman et al., 2007), which delayed the warming effect in the atmosphere. Quantifying the oceanic uptake is difficult as C_{ant} cannot be directly measured. Different methods have been developed to estimate C_{ant} and regions of increased storage have been identified (e.g., Sabine and Tanhua, 2010).

The tropical Atlantic Ocean is affected by a multitude of zonal currents. Induced by the trade winds a westward surface water current, the Equatorial Current, is found at the equator and is accompanied by poleward Ekman transport north and south of the equator. This leads to upwelling along the equator associated with lower water temperatures. The so called 'cold tongue' develops in northern summer, when the trade winds are strongest. The poleward flowing surface waters lose contact with the atmosphere when they reach the subduction zones of the Subtropical Gyres and return back to the equator at depths around 300–500 m (Schott et al., 2004). These shallow overturning circulations are named the Subtropical Cells. The southern Subtropical Cell is intensified due to the Meridional Overturning Circulation, which transports warm water towards the north in the North Brazilian Undercurrent. Below the westward flowing Equatorial Current, the Equatorial Undercurrent flows in the opposite direction, together with the North and the South Equatorial Undercurrents at around 5°N and 5°S, respectively. A cyclonic circulation in the shadow zone south and southeast of the northern Subtropical Gyre causes the permanent, quasi-stationary Guinea Dome (Siedler et al., 1992), which is mainly fed by the North Equatorial Undercurrent (Schott et al., 2004). Ekman upwelling occurs both, in the Guinea Dome and along the coast. Similar features are found south of the equator.

* Corresponding author.
E-mail address: aschneider@geomar.de (A. Schneider).

0967-0637/$ - see front matter © 2012 Elsevier Ltd. All rights reserved.
http://dx.doi.org/10.1016/j.dsr.2012.05.007

The intermediate and deep zonal currents in the equatorial region are influenced by water masses originating in both the northern and the southern hemisphere. These are the North Atlantic Deep Water (NADW) coming from the north as part of the Deep Western Boundary Current and the Antarctic Intermediate Water (AAIW) coming from the south along the South American continent. At low latitudes both water masses are partly deflected towards the east and can be observed along the equator. The NADW is separated into the upper and the lower NADW, which both show increased chlorofluorocarbon (CFC) concentrations (Weiss et al., 1985; Rhein et al., 1995; Rhein and Stramma, 2005).

The upwelling regions in the tropical Atlantic Ocean might play a considerable role in the C_{ant} uptake because in upwelling regions old water comes up to the surface. Due to remineralization of organic matter this water has increased inorganic carbon concentrations and thus is a source of CO_2 for the atmosphere. However, at the same time it is a sink for anthropogenic CO_2 because the magnitude of the CO_2 source has decreased, due to higher atmospheric CO_2 concentrations compared to conditions in the upwelling zone during preindustrial times. The water, which comes up to the surface in the equatorial upwelling region, is a mixture of the water masses participating in the Subtropical Cells (within the upper 500 m). However, deeper water masses can be picked up at the lower boundary and participate in the circulation. Of major interest for the C_{ant} uptake is the contribution of water that lost contact with the atmosphere longtime ago and therefore shows little or even no contamination with anthropogenic CO_2. This could be the case for AAIW, that has been circulated around the southern Subtropical Gyre before entering the equatorial region (Warner and Weiss, 1992; Stramma and Schott, 1999) and for Indian Central Water brought into the Atlantic Ocean by the Agulhas Current (Tomczak and Godfrey, 1994).

The aim of this study was to investigate ventilation processes in the tropical North Atlantic region as well as to quantify C_{ant} concentrations and inventories. To achieve these objectives a project to measure tracers with good spatial coverage and with high vertical sampling density was designed. On several recent cruises to the eastern tropical Atlantic, dichlorodifluoromethane (CFC-12) and sulfur hexafluoride (SF_6) concentrations were determined. With the help of these tracer measurements the mean ages and C_{ant} concentrations are estimated and the differences between water masses and between regions are highlighted. Further, the column inventories of anthropogenic carbon of all sampled stations are determined and the total C_{ant} inventories of the equatorial and the Guinea Dome regions are estimated.

2. Methodology

2.1. Water samples

Between 2006 and 2009 four cruises were undertaken to the tropical Atlantic. Three cruises with the R/V Meteor (M68/2 in 2006 and M80/1 and M80/2 in 2009) and one cruise with the R/V Maria S. Merian (MSM10/1 in 2008). The stations of the four cruises that were sampled for tracers are shown in Fig. 1. Cruises MSM10/1 and M80/2 were part of a tracer release experiment. This explains the unique cruise tracks and the high sampling density. Altogether almost 6000 CFC-12 and 1200 SF_6 samples were analysed. Generally, the upper 1000–1500 m of the water column were sampled, with some additional deep stations. Most samples were measured onboard and only

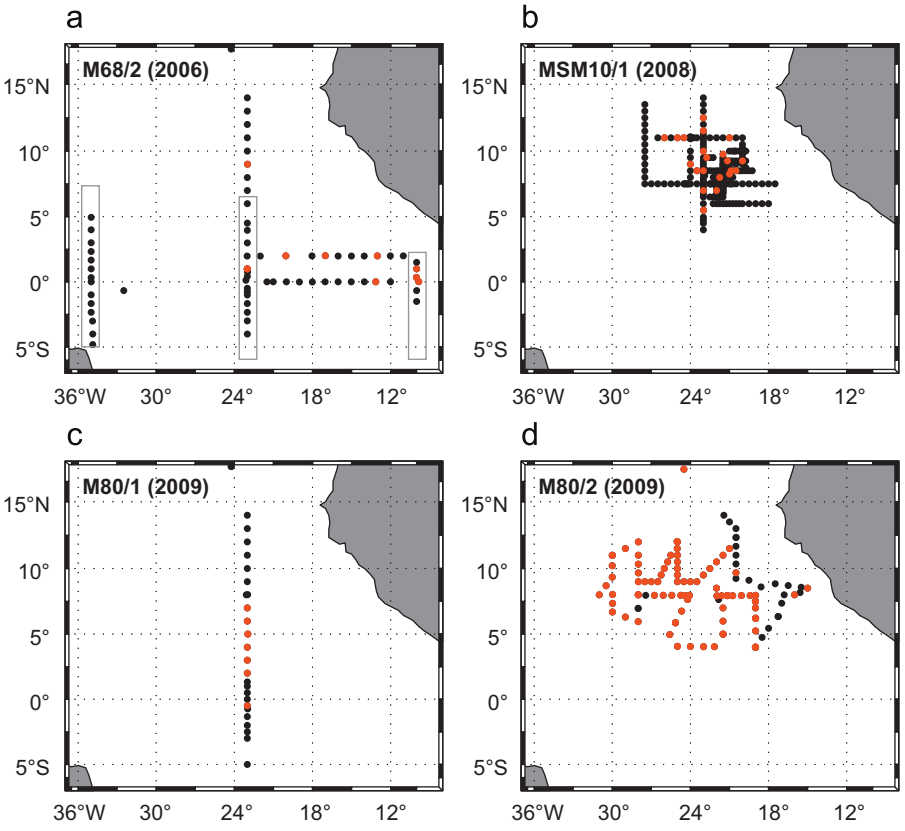

Fig. 1. Sampled stations of all cruises to the tropical Atlantic. Red dots indicate the stations where SF_6 was measured additionally to CFC-12. On map (a) three sections that were sampled for trichlorofluoromethane (CFC-11) in the year 1999 are highlighted with grey (Touratier et al., 2005). (For interpretation of the references to color in this figure caption, the reader is referred to the web version of this article.)

a subset of about 100 samples were flame sealed and taken back for shore-based analysis.

Two slightly different purge and trap systems, both connected to gas chromatography - electron capture detector systems, were used for the tracer analysis. The first one (system A) is a system similar to that described by Bullister and Weiss (1988) and is not suitable for measuring SF_6, mainly because cooling of the trap is achieved with Peltier elements reaching minimum temperatures at −45 to −50 °C. For quantitative detection of SF_6 temperatures of about −60 °C are necessary. Samples for system A are collected in glass syringes and are measured directly onboard. The second system (system B) uses liquid nitrogen for cooling of the trap to −60 °C and thus CFC-12 and SF_6 can be trapped simultaneously. Samples are collected in glass ampoules and can be measured directly onboard or be flame sealed for later analysis. The precolumn of system B is 30 cm of 1/8 in stainless steel tubing packed with Porasil C. The main column is 2 m of 1/8 in stainless steel tubing packed with 180 cm Carbograph and 20 cm molecular sieve 5 Å. During one cruise (MSM10/1 in 2008) capillary columns instead of packed columns were used for the gas chromatographic separation (system B^*). The precolumn used for system B^* is a 1/8 in stainless steel tubing packed with 50 cm Porasil C and 50 cm molecular sieve 5 Å. The main column is a combination of two capillary columns arranged in series. The first is a 75 m DB 624 and the second is a 30 m RT-molecular sieve 5 Å.

In Table 1 information about the analysis and the errors for all cruises is summarized. The systematic errors combine measurement blanks and errors originating from the analysis. The precision is given in fmol kg^{-1} and %, whichever is greater. In parenthesis the number of duplicates is given. A standard problem during M80/1 and M80/2 resulted in too low values and an additional adjustment factor of 1.09 was applied to the onboard CFC-12 measurements on system B.

For direct comparison with the atmospheric mixing ratios, the measured tracer concentrations are converted into equivalent mixing ratios, which are calculated as

$$\text{Equivalent mixing ratio} = \frac{c}{F(T,S)\cdot(P_{\text{atm}} - P_{H_2O}(T,S))}, \quad (1)$$

where c is either the CFC-12 or the SF_6 concentration in pmol kg^{-1}, $F(T,S)$ is the temperature and salinity dependent solubility function for each of the gases in mol kg^{-1} atm^{-1} (Warner and Weiss, 1985; Bullister et al., 2002), P_{atm} is the mean atmospheric pressure in atm and $P_{H_2O}(T,S)$ is the temperature and salinity dependent partial pressure of water vapor (Weiss and Price, 1980).

2.2. Anthropogenic carbon calculation

Using the Transient Time Distribution (TTD) method together with tracer measurements, the mean age and the anthropogenic carbon concentration can be estimated. The TTD method assumes that a water parcel consists of waters with varying time histories. Instead of a single age, each water parcel has an age—or transit time distribution. Using the measured transient tracer concentration together with its atmospheric time history, the TTD and mean age can be determined for each water sample. The interior concentration $c(t)$ of the tracer at time t is given by Hall and Plumb (1994)

$$c(t) = \int_0^\infty c_0(t-t')\cdot G(t')\,dt', \quad (2)$$

where $c_0(t-t')$ is the surface water tracer concentration in the year $t-t'$. $G(t')$ is the TTD, which can be approximated for steady transport by an inverse Gaussian function (Waugh et al., 2004), that is:

$$G(t') = \sqrt{\frac{\Gamma^3}{4\pi\Delta^2 t'^3}}\cdot\exp\left(\frac{-\Gamma(t'-\Gamma)^2}{4\Delta^2 t'}\right), \quad (3)$$

where Γ is the mean transit time ('mean age') and Δ defines the width of the TTD.

Further, in combination with the atmospheric histories of CO_2 and an empirical regional alkalinity-salinity correlation, the anthropogenic carbon content can then be estimated as follows:

$$C_{\text{ant}}(t) = \int_0^\infty C_{\text{ant},0}(t-t')\cdot G(t')\,dt', \quad (4)$$

where t is the sampling year.

For the TTD calculations 100% saturation has been assumed for surface waters with respect to CFC-12 and SF_6. The atmospheric time history of SF_6 was taken from Maiss and Brenninkmeijer (1998) combined with measurements made since 1995 by the National Oceanic & Atmospheric Administration (NOAA/ESRL, 2011). For CFC-12 the atmospheric time history from Walker et al. (2000) was used and continued from 1998 onwards with measurements from the National Oceanic & Atmospheric Administration (NOAA/ESRL, 2011). Given that waters in the equatorial Atlantic have their origin in both hemispheres, a global mean was used for the atmospheric time histories of both tracers. The past CO_2 concentrations in the atmosphere are merged from reconstructions from the Law Dome ice core (Etheridge et al., 1996) and since 1959 from direct measurements at the Mauna Loa, Hawaii (Tans, 2011). The method allows for spatial variations in the CO_2 disequilibrium between surface waters and the atmosphere but a constant CO_2 disequilibrium over time has been assumed. The surface alkalinity-salinity relationship in the tropical region, used to convert the anthropogenic part of the atmospheric carbon mixing ratios (in ppt) into dissolved anthropogenic carbon concentrations (in µmol kg^{-1}), was determined from total alkalinity (A_T) and salinity measurements during the M68/2 and M80/1 cruises ($A_T = 66.7(\pm 1.1)\cdot S - 45.9(\pm 39.2)$ µmol kg^{-1}; $r^2 = 0.96$).

Table 1
Analytical details of all tracer measurements.

Cruise	Tracer	System	Analysis	Systematic errors[a] (fmol kg^{-1})	Precision (fmol kg^{-1})/(%) (n)
M68/2	SF_6	B	Shore-based	–	– (0)
	CFC-12	A	Onboard	−3	–/±1.4 (190)
MSM10/1	SF_6	B^*	Onboard	−0.05	–/±2.2 (1)
	CFC-12	A	Onboard	–	±10.8/±1.9 (541)
M80/1	SF_6	B	Onboard	−0.08	– (0)
	CFC-12	B	Shore-based	−2.8	– (0)
	CFC-12	B	Onboard	–	±50/±6 (4)
M80/2	SF_6	B	Onboard	–	±0.05/±10 (13)
	CFC-12	A	Onboard	–	±6/±1 (46)
	CFC-12	B	Onboard	–	±40/±3.8 (13)

[a] Measured blanks and analytical errors combined.

The ratio of the constants Δ and Γ in the inverse Gaussian function parameterises the relative importance of mixing over advection. A larger ratio implies stronger mixing. For ocean interior waters it has been shown, that the usage of a Δ/Γ ratio of 1 is appropriate (Waugh et al., 2004). Whether this value for the ratio is appropriate for the tropical Atlantic waters studied here had not been tested yet. However, on the basis of two transient tracers with differing atmospheric time histories, e.g. CFC-12 and SF_6, the appropriate Δ/Γ ratio can be approximated, as described in Section 3.1.

3. Results and discussion

In the following, error ranges (ER) are added to the C_{ant} estimates. The error ranges result from upper and lower limits of the assumptions made for the TTD calculations and are further explained in the appendix.

3.1. Tracers and the Δ/Γ ratio

To evaluate the Δ/Γ ratio, the C_{ant} concentrations are determined initially based on CFC-12 measurements and a second time based on SF_6 measurements using the same Δ/Γ ratio of 1. In Fig. 2 the consistent C_{ant} estimates from CFC-12 and SF_6 are plotted against each other. They basically follow the one to one relation (highlighted with a black line), indicating that the chosen Δ/Γ ratio of 1 is applicable for the upper 1500 m in the tropical Atlantic. Colour coded are the CFC-12 concentrations in ppt. At low CFC-12 concentrations the scatter increases, because these data are close to the detection limit of SF_6. At high CFC-12 concentrations (younger waters) a deviation of the data from the one to one line is apparent. Our hypothesis is, that this deviation is caused by the decreasing gradient in the atmospheric CFC-12 concentrations, which is reflected in the water concentrations in Fig. 3a and which makes it difficult to determine the appropriate age and corresponding C_{ant} concentration. Tanhua et al. (2008) found, that for waters exceeding $\sim$450 ppt, the uncertainty in the CFC-12 based C_{ant} estimates increases. This limit seems to be in agreement with our data, as the data points greater than 450 ppt in CFC-12 are the ones varying from the linear relationship.

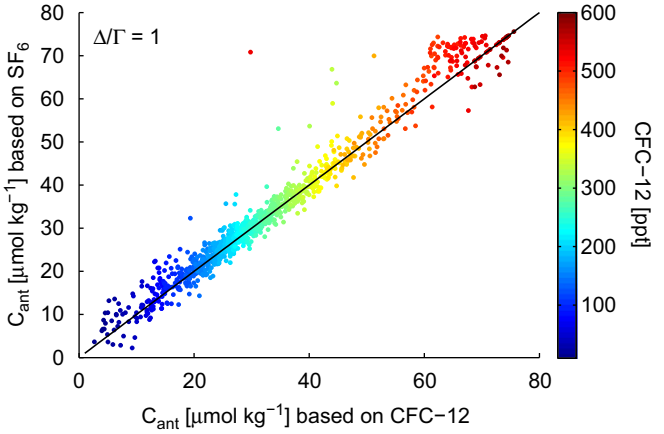

Fig. 2. The SF_6 based C_{ant} estimates are plotted against the CFC-12 based C_{ant} estimates. For both estimates a Δ/Γ ratio of 1 has been used. Colour coded are the CFC-12 concentrations in ppt. The black line indicates a one to one relation.

Fig. 3a and b shows the depth profiles of CFC-12 and SF_6 in µmol kg^{-1} and in ppt. In the upper 100 to 200 m, where CFC-12 samples exceed 450 ppt, indicated by the magenta line, a pronounced vertical gradient can be seen in the SF_6 data but is absent from the CFC-12 profile. Therefore, samples with CFC-12 concentrations between 450 and 540 ppt, the SF_6 measurements are used to calculate the C_{ant} concentrations, as they allow calculation of a unique TTD. Where no SF_6 measurements were available, a transfer function was applied to the CFC-12 based C_{ant} estimates. This function ($y = 1.2 \cdot x - 10.7$) was determined by linear correlation between all existing pairs of SF_6 based and CFC-12 based C_{ant} estimates for samples with CFC-12 concentrations between 450 and 540 ppt (Fig. 3c). In effect, this function forces the data to follow the one to one relationship in Figs. 2 and 3c. All samples with CFC-12 concentrations greater than 540 ppt are assumed to be recently ventilated and the water age is set to zero, which means that the C_{ant} concentrations are only dependent on the contemporary C_{ant} mixing ratios in the atmosphere and on the carbonate system parameters.

3.2. Hydrography and vertical profiles

The main water masses in the region can be identified with the help of a temperature-salinity (T–S) diagram, shown together with the isopycnals in Fig. 4. The upper NADW and the AAIW have a potential density (σ_Θ) of 27.75 kg m^{-3} and 27.3 kg m^{-3}, respectively. Both water masses are clearly defined in the stations of the equatorial band (5°S - 5°N), highlighted in red. The Central Water (CW) with a core density of 26.5 kg m^{-3} extends almost linear across the T–S diagram. South of 15°N the origin of the CW lies mainly in the South Atlantic (Stramma and Schott, 1999).

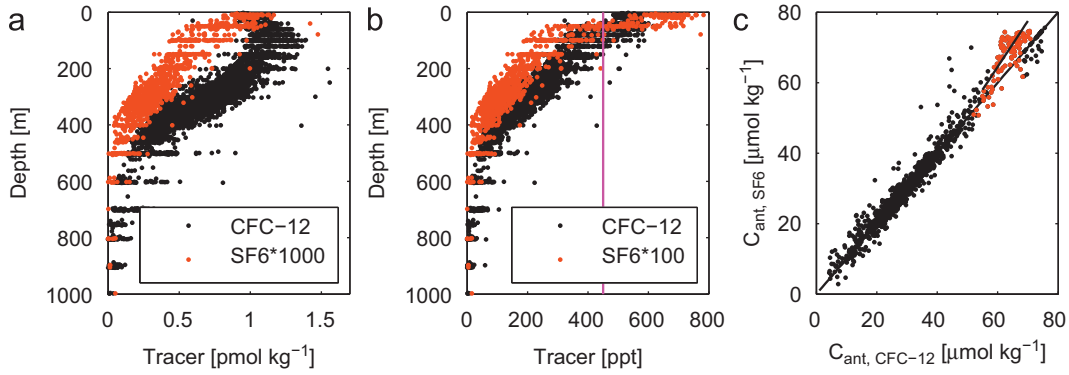

Fig. 3. (a) and (b) show depth profiles of the CFC-12 (black) and SF_6 (red) measurements from all cruises to the tropical Atlantic. (a) The tracer concentrations in pmol kg^{-1}, where the SF_6 values are multiplied by 1000. (b) The tracer equivalent mixing ratios in ppt, where the SF_6 values are multiplied by 100. The magenta line indicates the CFC-12 border of 450 ppt. (c) The SF_6 based C_{ant} estimates plotted against the CFC-12 based C_{ant} estimates. Data points with CFC-12 concentrations between 450 and 540 ppt are highlighted in red and the transfer function is illustrated. (For interpretation of the references to color in this figure caption, the reader is referred to the web version of this article.)

The South Atlantic Central Water (SACW) is described as a straight line between the *T–S* points 5 °C, 34.3 and 18 °C, 35.8 (Emery and Meincke, 1986) (Fig. 4, light grey bar). This is the same *T–S* curve as of the Indian and the Western South Pacific Central Waters (Tomczak and Godfrey, 1994). According to Tomczak and Godfrey (1994) part of the SACW is, in fact, Indian Central Water. The *T–S* line of North Atlantic Central Water (NACW) is found at higher salinities (Emery and Meincke, 1986) (Fig. 4, dark grey bar). The reason why samples of the CW in the *T–S* diagram north of 5 °N have higher salinities is that SACW mixes with NACW, which could be brought to the Guinea Dome area by the North Equatorial Undercurrent. The 25.8 kg m^{-3} isopycnal represents the lower boundary of the Tropical Surface Water. Part of the Tropical Surface Water is the Salinity Maximum Water (Defant, 1936), which is characterized by a subsurface salinity maximum, while the overlying water is poor in salinity due to precipitation. Especially in the area of the Intertropical Convergence Zone (located at around 10°N in northern fall), the decreasing salinities are more pronounced (Fig. 4, samples north of 5°N, black dots).

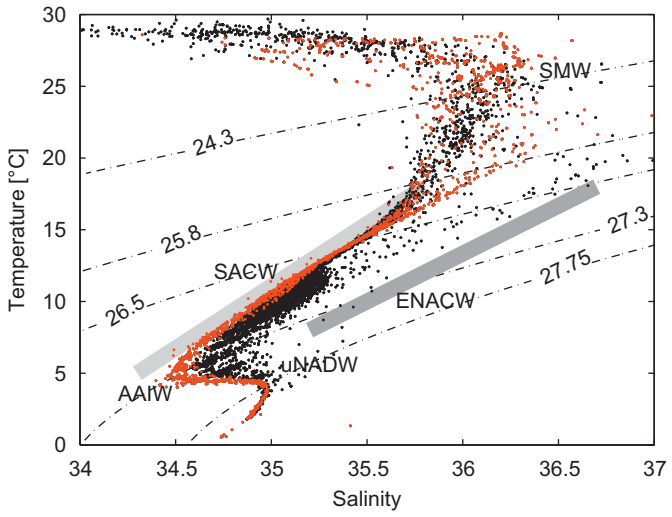

Fig. 4. *T–S* diagram of all sampled stations in the tropical Atlantic. Some characteristic water masses described in the text can be identified with the help of isopycnals (potential density in kg m^{-3}). The Antarctic Intermediate Water (AAIW), the upper North Atlantic Deep Water (uNADW) and the Salinity Maximum Water (SMW). The light and the dark grey bars indicate the salinity-temperature characteristics of the South Atlantic Central Water (SACW) and the eastern North Atlantic Central Water (ENACW) after Emery and Meincke, 1986. Red dots indicate the stations located in the equatorial region between 5°N and 5°S. (For interpretation of the references to color in this figure caption, the reader is referred to the web version of this article.)

Fig. 5 shows the depth profiles of oxygen, mean age and anthropogenic carbon over the entire water column. The vertical oxygen distribution (Fig. 5a) illustrates the pronounced oxygen minimum zone found between 400 and 500 m. Lowest oxygen concentrations are about 40 μmol kg^{-1} and are far from being suboxic (oxygen concentrations of <4.5 μmol kg^{-1} are defined as suboxic Warren, 1994; Morrison et al., 1999). Comparing the oxygen profile with the profile of the mean age (Fig. 5b) demonstrates that the oxygen minimum lies about 600 m above an age maximum which is located in the AAIW and below at a depth of around 1000 m. Hence, the low oxygen concentrations seem to be the consequence of enhanced remineralization combined with increasing water age. The C_{ant} concentrations (Fig. 5c) are highest at the surface and decrease from maximum values of 71 μmol kg^{-1} (error range (ER): 69−−77 μmol kg^{-1}) in the upper 20 m down to about 3.5 μmol kg^{-1} (ER: 2.8–5.9 μmol kg^{-1}) at 1000 m depth. A relative C_{ant} maximum with concentrations up to 10 μmol kg^{-1} around 1800 m represents the upper NADW and at depths around 3700 and 4000 m a further maximum with slightly increased concentrations is found in the lower NADW.

In the year 1999 three N-S sections between 6°S and 7°N (see Fig. 1a, grey boxes), were sampled for oxygen, dissolved inorganic carbon, total alkalinity and trichlorofluoromethane (CFC-11). These sections match several stations sampled during the present study. Touratier et al. (2005) used measurements of oxygen, dissolved inorganic carbon and total alkalinity from the year 1999 to compute the C_{ant} concentrations from the so called 'Tracer combining Oxygen, inorganic Carbon and total Alkalinity approach' (TrOCA) (Touratier and Goyet, 2004). In order to check consistency, in the following we will compare C_{ant} estimates based on the TrOCA method with C_{ant} estimates based on the TTD method. Further, we will compare C_{ant} estimates using CFC-11 with estimates using CFC-12, both based on the TTD method.

We recalculated the C_{ant} concentrations for 1999 with the TrOCA approach (Touratier et al., 2005), using corrected data for dissolved inorganic carbon (+6 μmol kg^{-1}) and total alkalinity (−6 μmol kg^{-1}) suggested by Velo et al. (2009); Pierrot et al. (2010). Fig. 5c shows the results extended to the year 2007 (the mean sampling year of the present study), by assuming the same relative C_{ant} increase in the ocean as in the atmosphere (steady transport), in comparison to our C_{ant} estimates based on the TTD method. The C_{ant} estimates based on the TrOCA approach (grey) are about 10–20 μmol kg^{-1} higher than the estimates based on the TTD method and show much more scatter. Nevertheless, the

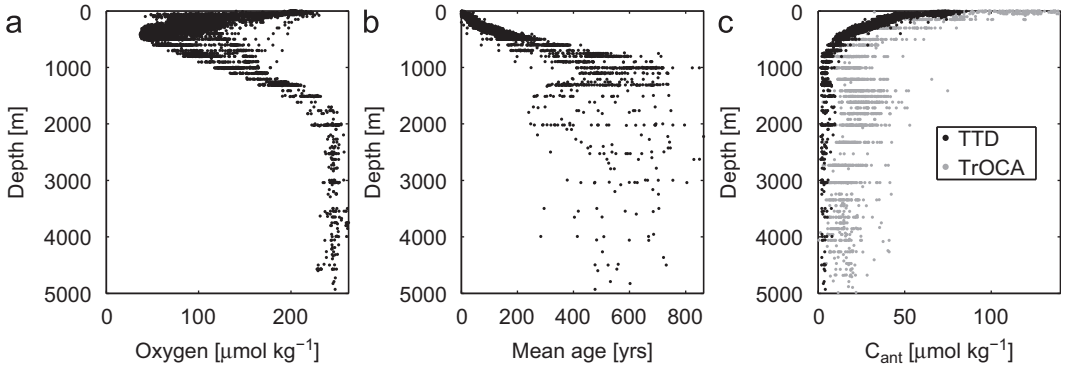

Fig. 5. Depth profiles over the entire water column of (a) oxygen, (b) mean age and (c) anthropogenic carbon. All samples from the cruises to the tropical Atlantic between 2006 and 2009 are shown in black. Grey dots show C_{ant} estimates by Touratier et al. (2005) based on the TrOCA method using measurements of oxygen, dissolved inorganic carbon and alkalinity from a cruise to the tropical Atlantic in 1999. For this plot the estimates were scaled to the year 2007 by assuming the same relative C_{ant} increase in the ocean as in the atmosphere.

C_{ant} profiles of both approaches have the same characteristics and show that the entire water column has been penetrated by C_{ant}.

The CFC-11 data from the year 1999 used by Touratier et al. (2005) have been corrected with a factor of 0.85 (Steinfeldt et al., 2010). A comparison of the CFC-11 measurements and the CFC-12 measurements from this study also exhibits the same characteristics in the water column. The two left hand side panels in Fig. 6(a) and (b) show the CFC-11 measurements made in 1999 and the CFC-12 measurements on the same sections from this work, respectively. CFC-11 is more soluble in sea water than CFC-12, which has lead to higher equilibrium concentrations of CFC-11 in surface water (Fig. 7a). However, the relation between the equilibrium concentrations is not constant because of the varying atmospheric histories of CFC-11 and CFC-12 (Fig. 7b). Consequently, CFC-11 concentrations are about twice as high in middle-aged waters and the CFC-11 to CFC-12 ratio decreases in older waters and somewhat in younger waters of the upper water column. The right hand side panel in Fig. 6a shows the C_{ant} estimates for the campaign in 1999 but this time calculated with the TTD method using the CFC-11 concentrations (grey dots for the year 1999 and black dots scaled to the year 2007). The right hand side panel in Fig. 6b again shows the C_{ant} estimates of the present study based on the TTD method using the CFC-12 concentrations. In both cases the same assumptions were used for the TTD approach. As the CFC-11 measurements exhibit more scatter than the CFC-12 measurements, this also leads to more scatter in the C_{ant} estimates based on CFC-11, but in general very good agreement is found between the C_{ant} estimates using the two tracers from different years.

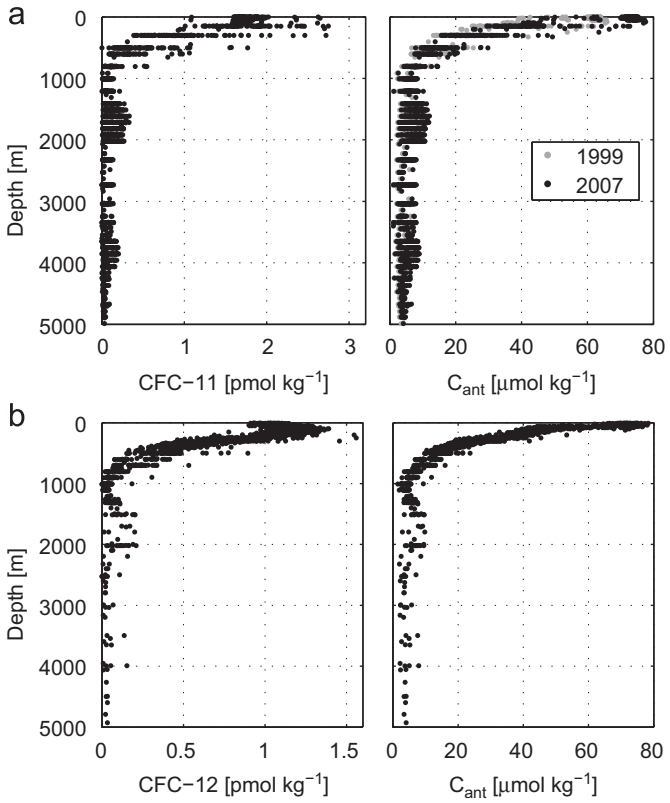

Fig. 6. (a) Vertical profiles of CFC-11 and C_{ant}. CFC-11 data are from measurements made on a cruise in 1999 to the tropical Atlantic (Touratier et al., 2005) and were used to estimate the C_{ant} concentrations with the TTD method (grey dots). Black dots show the C_{ant} estimates but scaled to the year 2007 for better comparison with the present work. (b) Vertical profiles of CFC-12 from the present work and C_{ant} estimates based on the TTD method using the CFC-12 data. Samples for CFC-11 (a) and CFC-12 (b) were both taken in an area between 6°S to 7°N and 36°W to 10°W.

3.3. Hydrographic sections

During the four cruises, which form the basis for this work, a considerable number of stations (70) has been occupied on an N-S section along 23°W and crossing the equator (14°N–4°S). The same section has been sampled for CFC-11 in 1999 (6°N to 6°S). We now examine the transient tracer data for the two time periods with the aim of quantifying changes in ventilation along the 23°W section between 4°S and 6°N. In Fig. 8 we have plotted the average mean age calculated with the TTD method using the CFC-12 data from the 2006–2009 surveys vs. potential density. We then predicted the CFC-12 concentration for 2007 using the CFC-11 data from 1999. If the ventilation is constant these two curves should be equal. Note that this analysis (i.e. the change in mean-age) is relatively insensitive to the choice of the Δ/Γ ratio (Waugh et al., 2003). It seems that the ventilation in the upper water column might have increased over this time-frame, i.e. the CFC-12 concentration in 2007 is higher than predicted using the 1999 TTDs. For the AAIW our analysis suggests a slower ventilation, which however is uncertain considering difficulties to accurately measure the low CFC concentrations found in this water mass.

All measurements in the upper 1500 m along 23°W from the four cruises between 2006 and 2009 have been combined to create the section plot of anthropogenic CO_2 in Fig. 9a. The fact that stations were sampled at the same latitudes on repeated cruises, the uncertainty in the measurements and temporal variation of the tracer concentrations (samples taken between 2006 and 2009) lead to occasional sharp breaks appearing in the contour plot.

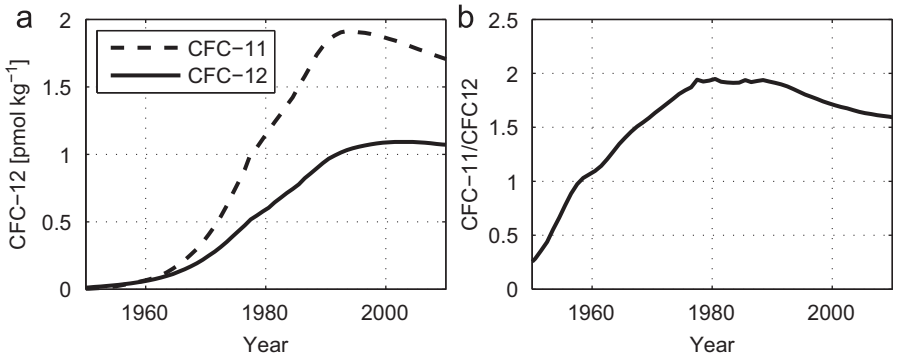

Fig. 7. (a) Estimated surface water equilibrium concentrations of CFC-11 and CFC-12 in pmol kg^{-1} at a temperature of 25°C over the past 60 years. (b) Ratio of the equilibrium concentrations over the past 60 years.

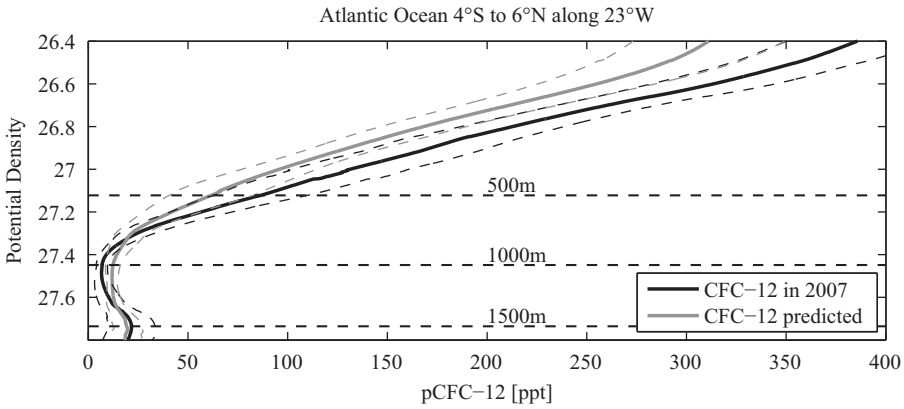

Fig. 8. Average profiles of the CFC-12 concentration for the section along 23°W (4°S–6°N) plotted vs. potential density. The black line is calculated using the 2006–2009 CFC-12 data (dashed lines denotes one standard deviation of the average profiles), and the grey line is the predicted CFC-12 concentration for 2007 using the TTDs determined with the 1999 CFC-11 data. Dashed horizontal lines are approximate depth horizons for comparison.

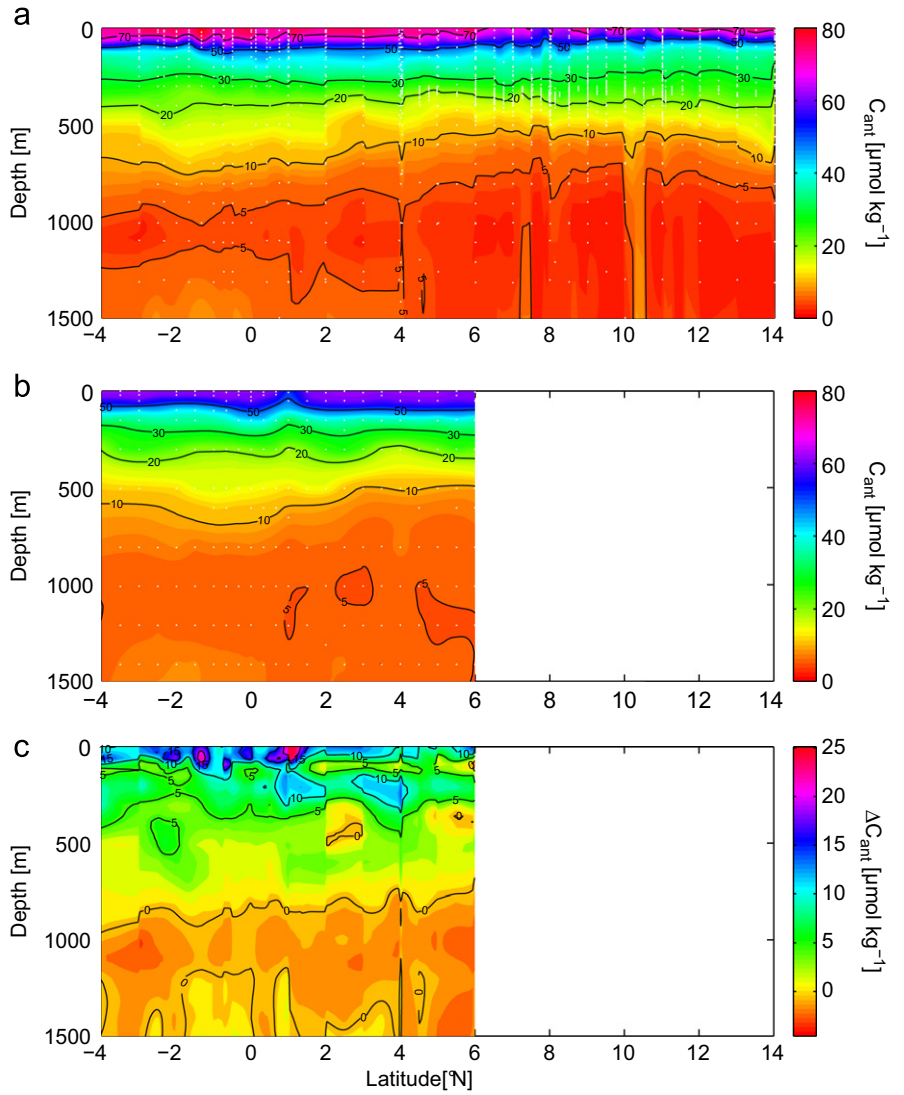

Fig. 9. Section plot of C_{ant} concentrations at 23°W. (a) TTD based C_{ant} estimates using CFC-12 and SF_6 measurements from 2006 to 2009. (b) TTD based C_{ant} estimates using CFC-11 measurements from 1999. (c) The difference (ΔC_{ant}) between the two estimates.

Highest C_{ant} concentrations are found in surface waters decreasing rapidly with depth. Mixed layer concentrations north of 6°N are up to 10 µmol kg^{-1} lower than south of 6°N. This could be due to temperature changes and to dilution by precipitation in the Intertropical Convergence Zone and a related change in the Revelle factor or to a different CO_2 disequilibrium. According to the C_{ant} depth profile a C_{ant} minimum is also observed around 1000 m on the 23°W section. These depths are occupied by AAIW

and Upper Circumpolar Water (a water mass located below the AAIW) (Oudot et al., 1999). In the northern hemisphere, concentrations below 10 μmol kg^{-1} seem to be extended over a wider depth range. Below 1000 m C_{ant} increases again due to the upper NADW, which brings younger water in the area.

In Fig. 9b the C_{ant} concentrations on the 23°W section in the year 1999 (estimated with the TTD method using CFC-11 measurements) are plotted against depth and reveal the same distribution pattern as in the years 2006–2009 (Fig. 9a). To illustrate the change in anthropogenic carbon during the 7–10 year period (mean 8.5 years), the concentrations were subtracted from each other. The resulting difference (ΔC_{ant}) is attributed to an increase in anthropogenic carbon. The ΔC_{ant} section is shown in Fig. 9c. The upper layer is characterized by the largest change and by a strong gradient. Down to 800 m a general C_{ant} increase can be observed but the distribution is very patchy, which could be caused by the zonal currents in the equatorial region.

The atmospheric increase in CO_2 between 1999 and 2007 is 15.6 ppm (Tans, 2011), which corresponds to an increase in dissolved inorganic carbon of ~9 μmol kg^{-1}. The TTD method assumes that the surface water keeps track of this increase. Deviations from this trend have to be due to changes in water mass properties (e.g. S and T) or increased upwelling. Our mean ΔC_{ant} values of 12.1 μmol kg^{-1} in the upper 60 m therefore suggest water mass changes in the area. In the AAIW at around 1000 m depth the ΔC_{ant} is zero or negative, which might be a consequence of analytical difficulties at low tracer concentrations. However, our analysis based on these data indicates that the ventilation of the AAIW has slowed down, explaining close to zero change in C_{ant}. In the upper NADW again an increase becomes apparent.

On a repeatedly sampled meridional Atlantic section A16 from Iceland to 56°S, decadal C_{ant} changes between 0 and 8 μmol kg^{-1} were found in the upper 1000 m of the low latitudes (Wanninkhof et al., 2010). Below that depth there was almost no change. The authors used an eMLR approach along density surfaces between cruises in 1989/1993 and 2003/2005, resulting in a rather smooth ΔC_{ant} distribution, which is in general agreement with the findings presented here. The patchiness in our data could be attributed to changes in oceanographic features with vertical structure, such as eddies, Rossby waves and movement of fronts, features normally 'neutralized' by the eMLR approach.

As described in 3.1 additional SF_6 measurements were used to estimate the C_{ant} concentrations or to correct the CFC-12 based C_{ant} estimates for recently ventilated waters, where CFC-12 becomes uncertain for age calculations. For the cruise in 1999 no additional tracer measurements are available, thus no corrections could be applied to the CFC-11 based C_{ant} estimates for recently ventilated waters (where also CFC-11 becomes uncertain for age calculations). However, in the tropics these corrections only apply to the surface layer and the effect is small. Furthermore, the atmospheric increase rate of the CFCs in the late 1990's were such that only a small correction is needed in the most recently ventilated waters. For example, in the upper 60 m the change in ΔC_{ant} would on average be reduced by 1.5 μmol kg^{-1}, when only non-corrected CFC-12 based C_{ant} estimates were used. No relevant change would be apparent below 100 m.

3.4. Density surfaces

The high vertical and horizontal sampling density between 15 - 30°W and 5–15°N (the area where the tracer had been released and referred to as 'patch' in the following) allows a detailed investigation of the area in comparison with the equatorial region. The mean age distribution and the anthropogenic carbon concentrations on different depth horizons are examined in order to identify regional variations. Four characteristic isopycnals were chosen. The potential density of 26.5 kg m^{-3} (100–200 m) is the core of the Central Water and the lower Equatorial Undercurrent. The core of the oxygen minimum zone (~400 m) is found at $\sigma_\Theta = 27.1$ kg m^{-3}, which is also the border between the CW and the AAIW. The AAIW (~800 m) has a potential density of 27.3 kg m^{-3}. As additional layer, $\sigma_\Theta = 26.85$ kg m^{-3} was chosen. This was the density where the tracer had been released and thus the sample density has been extremely high at that depth during the tracer hunt cruises.

In Fig. 10 the mean age and the C_{ant} concentrations are shown on the isopycnal layers. The CW exhibits relatively young mean ages of ~25−45 years and high C_{ant} concentrations (around 40 μmol kg^{-1}). Values towards the southwest are higher, which could be caused by the EUC. At $\sigma_\Theta = 26.85$ kg m^{-3} differences within the patch that seemed homogeneous in the CW layer are noticeable. Older waters are found in the southeastern part (difference of about 40 years) with corresponding lower C_{ant} concentrations, which could be caused by varying contributions (vertically and seasonally) of the North Equatorial Undercurrent and the North Equatorial Countercurrent in the area or to changes in the vertical density gradient, which have been identified in the same region and attributed to changes in the bottom topography (Banyte et al., 2012). The northwestern part of the patch and the equatorial region exhibit similar ages and C_{ant} concentrations.

Stronger differences between the equatorial and the northern region become visible with increasing depth (Fig. 10(e)–(h)). Younger waters are found in the oxygen minimum zone layer ($\sigma_\Theta = 27.1$ kg m^{-3}) and also in the AAIW layer ($\sigma_\Theta = 27.3$ kg m^{-3}) of the equatorial band. North of 15°N the water ages also seem to be younger than in the patch, but there are too few data to confirm this. In the AAIW layer very young waters are found close to the Brasilian coast, south of the equator. This is supposed to be the water coming from the south, moving towards the east at the equator. Along the equator, mean ages and C_{ant} concentration show a uniform distribution at all depths. Overall, Fig. 10 shows that water ages and C_{ant} concentrations vary considerably on the isopycnals.

Fig. 11 visualizes four different layers of the same mean age (isochrones) in a space spanned by longitude, latitude and depth. For the sake of clarity, the four isochrones are plotted in four separate panels. In addition, the depth variations are also highlighted by the color code. (Samples on the 34°W section have been left out.) The isochrones are (a) 15–20 years, (b) 60–65 years, (c) 120–130 years and (d) 220–230 years. In general, an elevation (decline) on an isochrone could be an evidence for upwelling (downwelling) or for the lateral inflow of older (younger) water. A defined elevation would also be expected in a region of reduced ventilation, where the water recirculates and the age increases. Here, in all four panels, a deepening of the isochrones towards the equator is apparent, which could be attributed to the strong zonal currents. Apart from that, panels (a) and (b) show a rather homogeneous pattern. The panel (c) (also visible in panel (b)) reveals two clear elevations centered at 5°N/22°W and 6°N/17°W, which are located in the area of the Guinea Dome and thus can be attributed to the upward displacement of the isopycnals in the dome. Siedler et al. (1992) localized the upper thermocline center of the dome at about 9°N/25°W in summer but mentioned that these positions are not well defined as they also found a double-cell structure. In the 220–230 years layer the Guinea Dome region is more homogeneous and the decline towards the equator is most pronounced.

Both, the Guinea Dome and the Equator are known as areas of regional upwelling. The well-established upward displacement of isopycnals in the Guinea Dome region can be identified in the isochrones as uplifting of older water (Fig. 11). In the equatorial

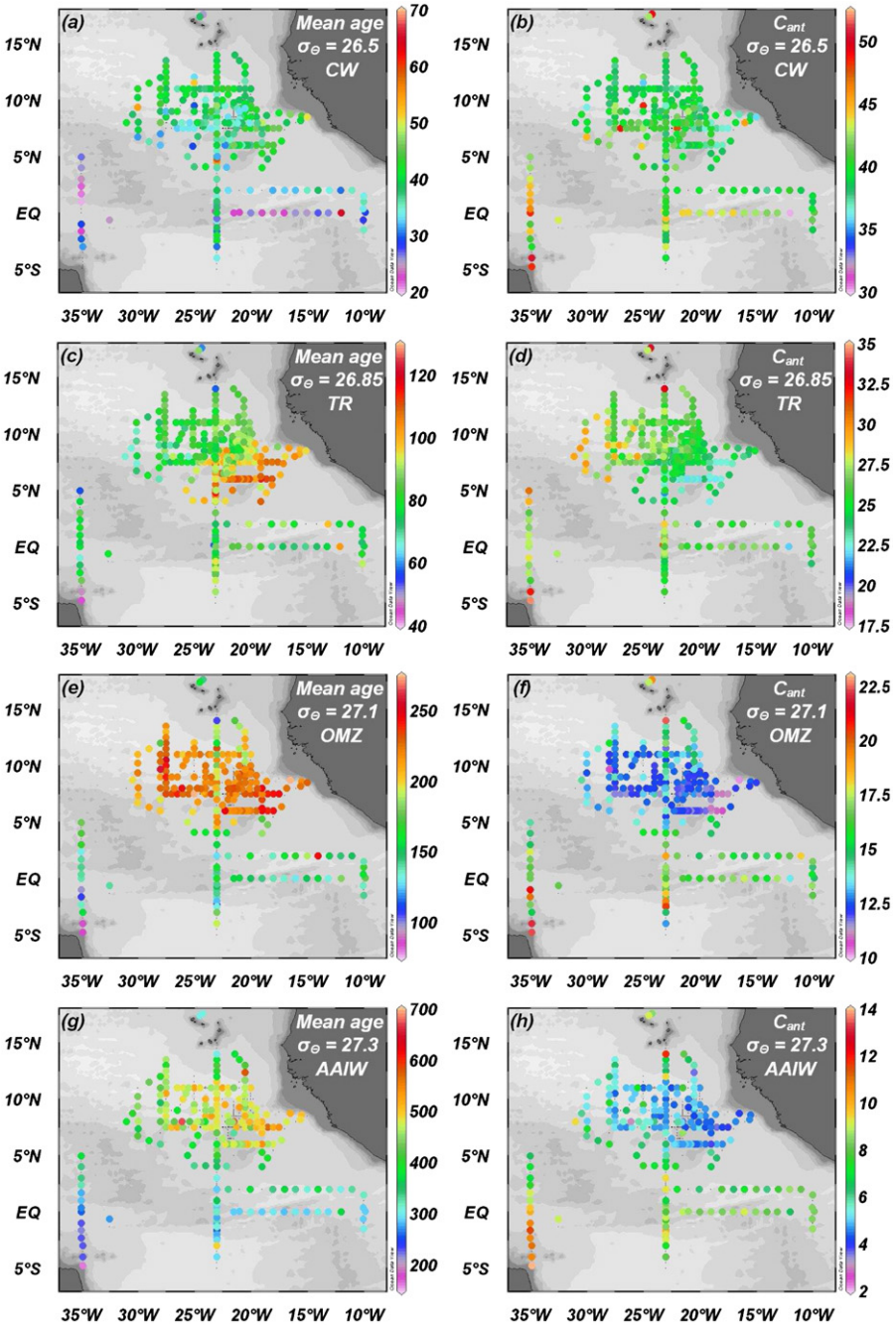

Fig. 10. Mean age (yr) and C_{ant} concentrations (μmol kg^{-1}) at characteristic potential densities (σ_Θ (kg m^{-3})). (a) and (b) Central Water, (c) and (d) Tracer release, (e) and (f) Oxygen minimum zone, (g) and (h) Antarctic Intermediate Water.

region the upwelling is rather a diffusive process that cannot be seen in the mean age distribution, due to the much stronger influence of the zonal currents that ventilate the area.

3.5. Inventories

3.5.1. Column inventories

Column inventories demonstrate regional differences in the amount of C_{ant} stored in the water column per square meter, depending also on the water depth. Fig. 12 shows the column inventories of the upper 1200 m of the tropical Atlantic. Below 1200 m the sample density is too poor to calculate distinct column inventories for each station. Between 5°S and 5°N the C_{ant} inventories are about 3 mol m^{-2} higher than north of 5°N. Next to the map in Fig. 12 the depth profiles of the C_{ant} concentrations north and south of 5°N are plotted to demonstrate from where the differences arise. At the depth range from the surface to 250 m and from 450 m to 1200 m the C_{ant} concentrations in the equatorial band are slightly higher than north of 5°N. This leads to overall higher column inventories. Between 250 m and 450 m C_{ant} concentrations are the same on average.

Column inventories over the entire water column (down to the bottom) have been estimated with mean C_{ant} values below 1200 m, due to the sampling sparseness at depth. The mean values at depth are averaged values from the stations where deep measurements are available. The maximum column inventory was 42 mol m^{-2} (ER: 39.4–56.3 mol m^{-2}) and the minimum column inventory was 23 mol m^{-2} (ER: 21.4–29.3 mol m^{-2}).

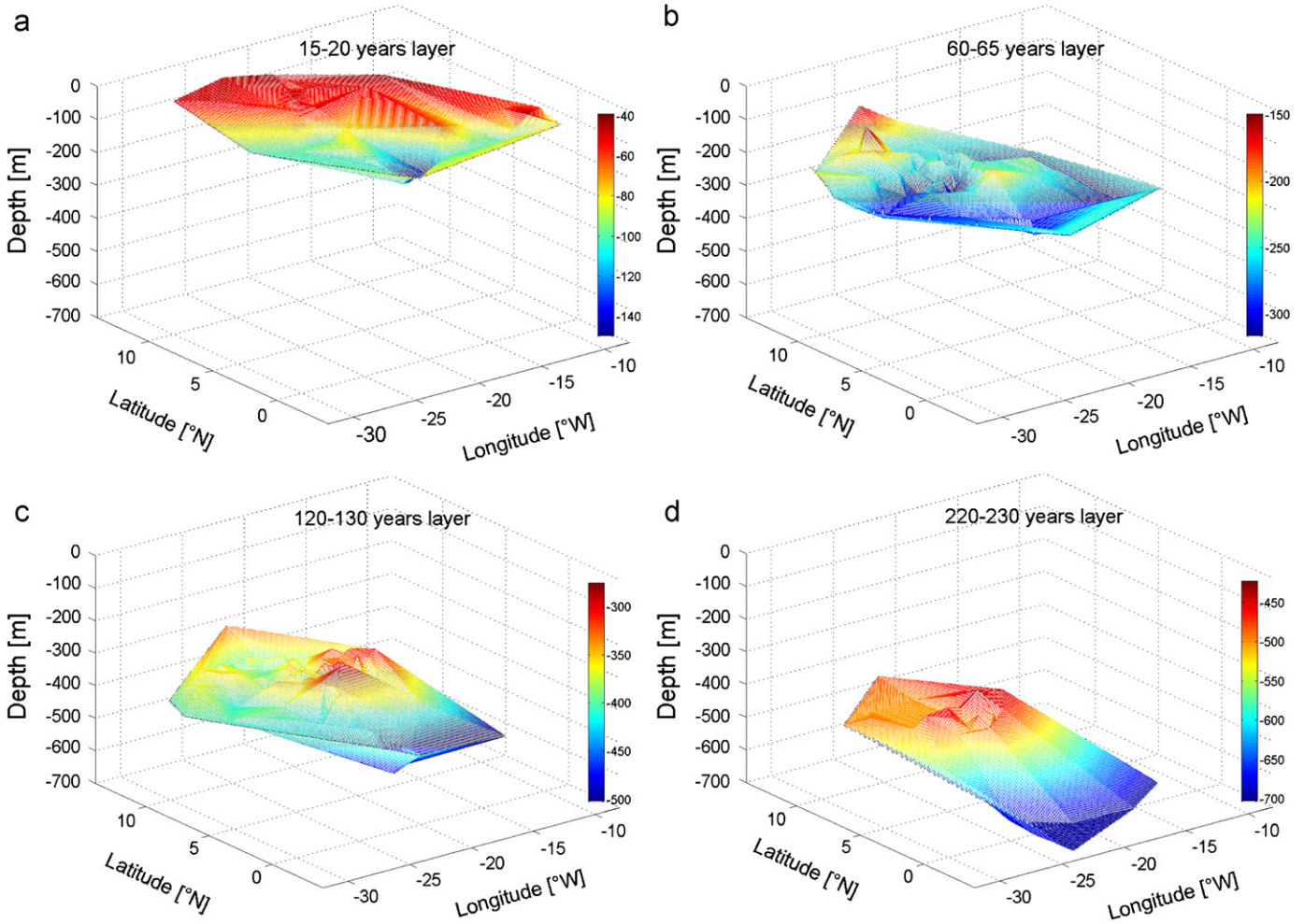

Fig. 11. Four isochrones (layers of the same mean age) are plotted against water depth in the sampling area. The colour code illustrates the relative depth variations for each isochrone.

The mean value for the entire column inventories in the tropical Atlantic is 32.2 mol m^{-2} (ER: 30.6–45.2 mol m^{-2}). Like in the upper 1200 m higher column inventories are found at the equator.

Column inventories estimated by Gruber (1998) (based on the ΔC^* method) for the latitude belt from the equator to 10°N in the year 1982 gave a mean value of 29 mol m^{-2}. The global C_{ant} column inventory maps by Waugh et al. (2006) (based on the TTD method) and by Sabine et al. (2004) (based on the ΔC^* method) for a mean sampling year of 1994 both show column inventories around 40 mol m^{-2} in the tropical region. Scaling these estimates to the year 2007 (assuming steady transport) gives mean column inventories of 49 mol m^{-2} and 52 mol m^{-2}, respectively. Both values are higher than our estimated mean column inventory of 32.2 mol m^{-2}, though they are close to the upper limit of our error range (45.2 mol m^{-2}). Given that mapping errors are not included in the error ranges, further discrepancies between the different studies can arise from the vertical mapping and the bottom depths chosen to determine the integrated C_{ant} values.

Further, the higher column inventories around the equator compared to the Guinea dome region found in the present work, is not evident in the global column inventory maps by Sabine et al. (2004) and Waugh et al. (2006). It is even reversed in the map by Waugh et al. (2006), where the authors find higher C_{ant} column inventories in the Guinea dome region compared to the equatorial band. However, when plotting the individual column inventories of the stations that were used to create that global map, the same trend as in Fig. 12 becomes visible. This shows that the gridding used for global maps can lead to false impressions and that discrete sampling is necessary.

3.5.2. Total inventory

A total C_{ant} inventory has been calculated for the area between 8 and 36°W and 4.5°S and 15°N. The size of the area is 6×10^6 km^2 and contains a total water volume of 25×10^6 km^3. The total inventory has been determined to be 2.5 Pg (ER: 2.3–3.5 Pg) of anthropogenic carbon. At depth, where no data of C_{ant} are available, a concentration of 3.2 μmol kg^{-1} was assumed. This is the mean value of all samples at depths between 2700 m and 3200 m and below 4100 m, where no direct influence of the upper NADW and the lower NADW is evident. According to Waugh et al. (2006) 50% of the C_{ant} content is generally found in the upper 500 m and 75% in the upper 1500 m. In our estimates for the tropical Atlantic, the percentages found are 50% and 66%), probably because the NADW at the equator contributes to increased C_{ant} values at depth.

By reason of the regional differences in water mass ages and the associated C_{ant} concentrations and column inventories discovered in Sections 3.4 and 3.5.1, the study area is partitioned into two regions of same size. One spanning 4.5° north and south of the equator and the second one from 4.5 to 15°N, each with an area of 2.8×10^6 km^2. The zonal extension is 11–36°W for both. For these two regions the total C_{ant} inventory turned out to be

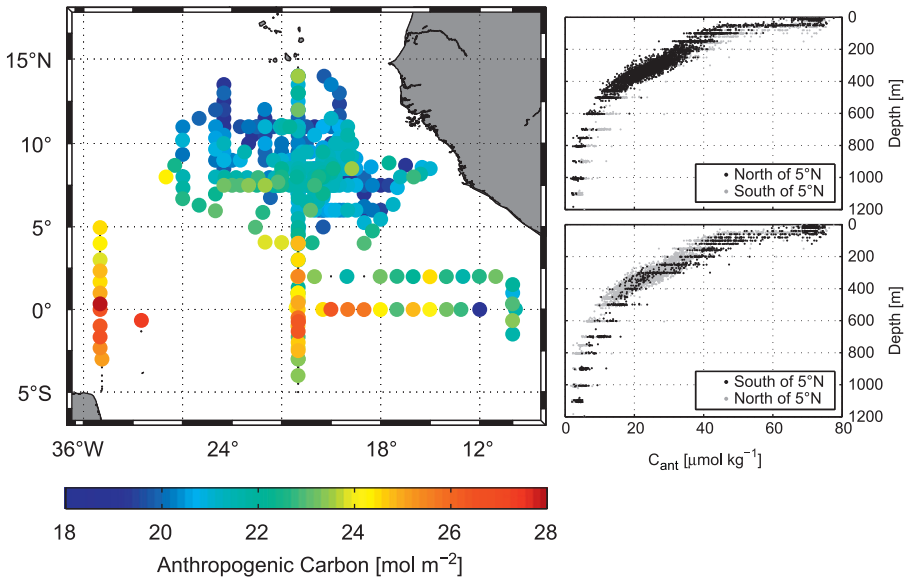

Fig. 12. Column inventories of the upper 1200 m for all sampled stations. On the right hand side the C_{ant} concentrations are indicated with black dots in the depth profiles for the areas from 5°S to 5°N (bottom) and from 5 to 15°N (top). The grey dots in the profile show the respective C_{ant} concentrations of the opposite area.

1 Pg (ER: 0.9–1.5 Pg) in the northern part and 1.4 Pg (ER: 1.2–1.8 Pg) in the southern part. This comparison shows that the eastern equatorial band has an C_{ant} inventory increased by 40% compared to an area of same size north of it.

Gruber (1998) estimated an Atlantic C_{ant} inventory from the equator to 10°N of 2.3 Pg C in the year 1982. For the same area our C_{ant} estimates gave an inventory of 2.5 Pg (ER: 2.2–3.5 Pg). Using the estimate by Gruber (1998) and extending it to the year 2007, would result in an inventory of 3.9 Pg of anthropogenic carbon in 2007, which is higher than our total inventory estimate for the same area.

4. Conclusions

The CFC-12 and SF_6 measurements from four cruises presented here together with the TTD method provide an extensive dataset of the mean age and C_{ant} distribution in the tropical Atlantic Ocean. The SF_6 measurements were used to a) improve the mean age estimates of waters with CFC-12 concentrations exceeding 450 ppt and b) to constrain a value of 1 for the Δ to Γ ratio, which is required for the TTD approach.

An analysis of mean age and C_{ant} distribution on isopycnals highlights differences between the equatorial belt and the Guinea dome north of it: (a) The mean age on an isopycnal decreases towards the south and the Guinea Dome area exhibits a pronounced local increase in mean age. (b) As a consequence, the C_{ant} concentrations are increased in the equatorial region compared to the Guinea dome area.

The column inventories in the upper 1200 m are on average 3 mol m^{-2} higher in the area from 5°S to 5°N than between 5° and 15°N. Mean column inventories over the entire water column are 32.2 mol m^{-2} (ER: 30.6–45.2 mol m^{-2}). The trend of higher inventories around the equator compared to the area north of it is also existent in the entire column inventories. Previous estimates of C_{ant} column inventories (Gruber, 1998; Sabine et al., 2004; Waugh et al., 2006) (scaled to the year 2007) do not show this trend and on average they are higher than the estimates presented here.

Calculation of the total inventory of anthropogenic carbon in the tropical Atlantic (for an area between 8 and 36°W and 4.5°S and 15°N) gave a value of 2.5 Pg (ER: 2.3–3.5 Pg). Dividing the area horizontally at 4.5°N reveals that the C_{ant} inventory in the equatorial belt is 40% higher than in the area north of it.

Measurements of CFC-11 in 1999 on an N-S section crossing the equator at 23°W from Touratier et al. (2005) were used to estimate C_{ant} concentrations with the TTD approach. The results are subtracted from the C_{ant} concentrations estimated on the same section as part of the present work and reveal a mean increase in anthropogenic carbon of 12.1 µmol kg^{-1} in the mixed layer for a period of 8.5 years. The transient tracer data indicate faster ventilation (in 2007 as compared to 1999) in the upper water column, but slower ventilation in the AAIW, that can explain changes in C_{ant} concentrations calculated with the TTD method with the two time periods. The TrOCA derived C_{ant} concentrations from 1999, however, are significantly higher as a result of being based on an entirely different method to calculate C_{ant}.

Acknowledgments

We thank Tina Schütt for helping with collection and measurement of the samples. Thanks also to the captain/crew and chief scientist of R/V Meteor and R/V Maria S. Merian for their assistance during all cruises. Funding for this work and the cruises was provided by the Deutsche Forschungsgemeinschaft (DFG) through grant WA 1434/10-1 and by the Sonderforschungsbereich (SFB) 754.

Appendix A. Uncertainty

In addition to the systematic errors in the tracer measurements, also the assumptions made for the TTD method produce uncertainty in the water mass ages and the anthropogenic carbon concentrations. In the following these assumptions are specified and realistic minimum and maximum values for the error calculation are given. As an example for the relative influence caused by the upper and lower limits of the assumptions and the precision, Fig. A.1 shows the respective uncertainties in the C_{ant} concentrations for the M80/2 cruise.

(1) In order to calculate TTDs based on the known atmospheric histories and the measured tracer concentrations, the saturation in surface waters at the time of water mass formation must be

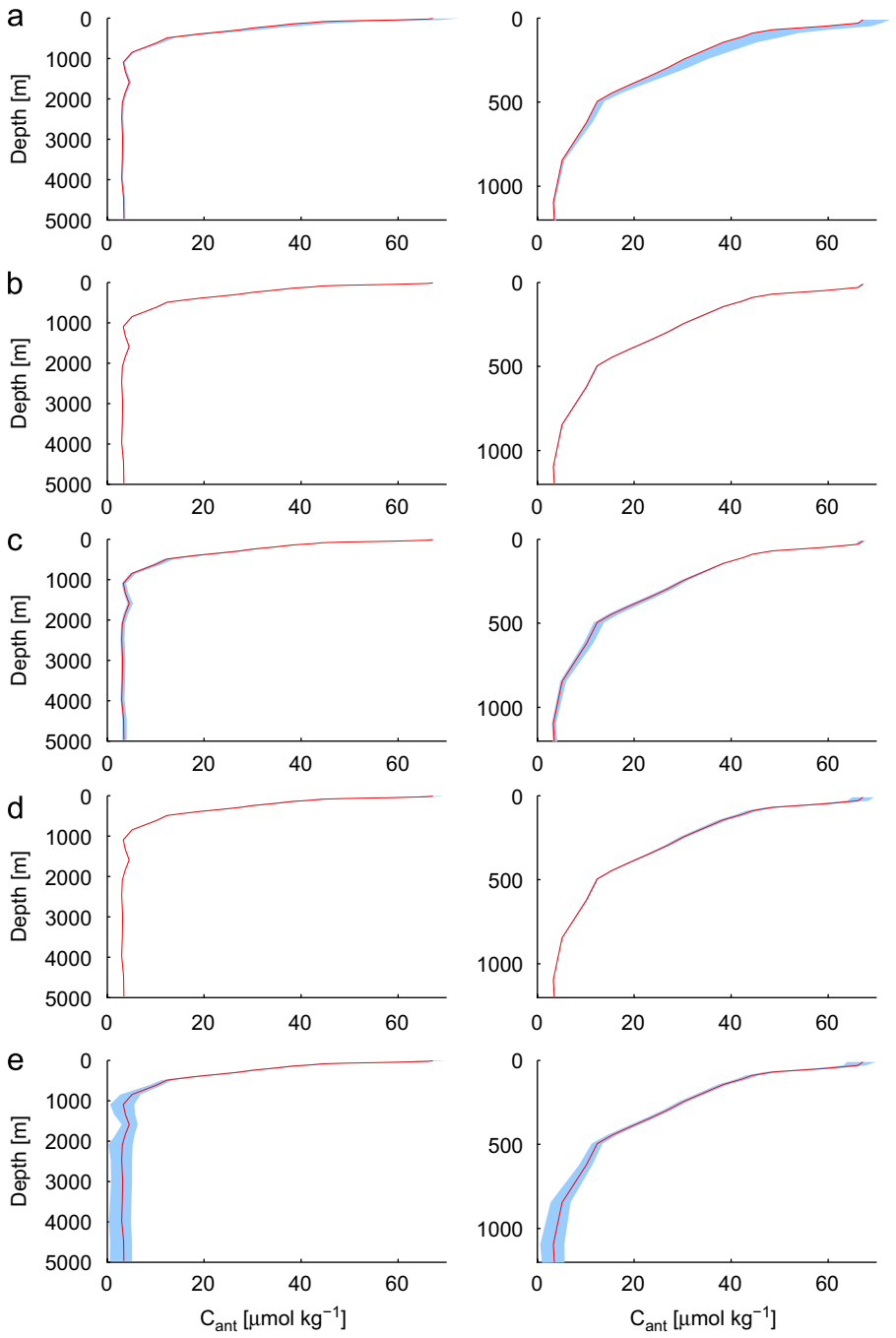

Fig. A.1. Mean C_{ant} profiles from M80/2 (red) plotted with the mean uncertainties (blue) resulting from the different sources of errors. On the right hand side the same profiles are shown for only the upper 1200 m. (a) A lower limit of 80% for the tracer saturation. (b) Atmospheric tracer time histories for the northern or the southern hemispheres. (c) Δ/Γ ratios of 0.75 and 1.25 (d) A linear changing CO_2 disequilibrium of $\pm 5\%$ in the last 110 years. (e) The determined precision of the tracer measurements. (For interpretation of the references to color in this figure caption, the reader is referred to the web version of this article.)

known. Here we assume 100% saturation with respect to the atmosphere for both tracers. Surface water samples of all cruises support this assumption as saturations were in the range from 98-103% in the tropics. For waters not originating in the tropics or subtropics, a lower saturation could be possible. This is especially likely in areas of deep convection, where water quickly cools and subducts before equilibrium with the atmosphere is reached (e.g. in the formation areas of the NADW and the AAIW), which would lead to higher C_{ant} estimates. As our lower limit for the tracer saturation a value of 80% was chosen. The impact of this on the C_{ant} concentrations is mainly seen in the upper 800 m, which means that the error in the upper NADW and in the AAIW is small (Fig. A.1 a). Saturations larger than 100% are not expected in subsurface waters as oversaturation generally only occurs in warm surface waters, which would not subduct due to the lower density.

(2) The sources of water in the tropical Atlantic are diverse and not restricted to one hemisphere. The atmospheric time histories of CFC-12 and SF_6 slightly differ for both hemispheres (lower concentrations are found in the southern hemisphere) and thus the boundary condition at the air-sea interface of the tracers depend on the origin of the water mass. Fig. A.1b shows that the uncertainty generated by using the different atmospheric time histories is insignificant.

(3) In Section 3.1 it has been shown that a Δ/Γ ratio of one seems applicable for the tropical Atlantic. Nevertheless it cannot be ruled out that water masses to some extend have experienced weaker or stronger mixing. Stronger mixing ($\Delta/\Gamma > 1$) results in increased ages and lower C_{ant} concentrations and weaker mixing ($\Delta/\Gamma < 1$) in younger ages and increased C_{ant} estimates. The limits for the error calculation were $\Delta/\Gamma = 0.75$ and $\Delta/\Gamma = 1.25$. As can be seen in Fig. A.1, stronger or weaker mixing has a considerable influence below 200 m.

(4) The TTD method assumes a constant CO_2 disequilibrium over time between surface waters and the atmosphere, which means that the strength of all natural CO_2 sources and sinks has remained constant. However, major changes in circulation and/or biological processescould invalidate this assumption. To account for such changes in the CO_2 disequilibrium a linear increase and decrease respectively by 5% from the year 1900 until the year 2010 was allowed in the error calculation. Only in the upper 500 m does changing CO_2 disequilibrium create a noticeable effect (Fig. A.1).

Comparing the size of the different errors on the C_{ant} estimates reveals that the precision of measurements makes up for large part of the uncertainty in water with low C_{ant} concentrations ($< 10\ \mu mol\ kg^{-1}$). In the upper water column the uncertainty is dominated by the influence of tracer undersaturation (which is not expected to be significant in the tropics) and the Δ/Γ ratio. The uncertainty generated by the different atmospheric tracer time histories in the northern and the southern hemispheres and the changing CO_2 disequilibrium is negligible. The given error ranges in the manuscript represent our estimates recalculated with the described limits resulting in negative and positive uncertainties, respectively.

References

Banyte, D., Tanhua, T., Visbeck, M., Wallace, D., Karstensen, J., Krahmann, G., Schneider, A., Stramma, L., 2012. Diapycnal Diffusivity at the upper boundary of the North Atlantic oxygen minimum zone. Journal of Geophysical Research; submitted for publications.

Bullister, J., Weiss, R., 1988. Determination of CCl_3F and CCl_2F_2 in seawater and air. Deep Sea Res. Part A. Oceanogr. Res. Papers 35, 839–853.

Bullister, J., Wisegarver, D., Menzia, F., 2002. The solubility of sulfur hexafluoride in water and seawater. Deep Sea Res. Part I. Oceanogr. Res. Papers 49, 175–187.

Defant, A., 1936. Schichtung und Zirkulation im Atlantischen Ozean. Die Troposphre. Wissenschaftliche Ergebnisse der Deutschen Atlantischen Expeditione "Meteor" 1925–1927 6, 289–411.

Denman, K., Brasseur, G., Chidthaisong, A., Ciais, P., Cox, P., Dickinson, R., Hauglustaine, D., Heinze, C., Holland, E., Jacob, D., Lohmann, U., Ramachandran, S., da Silva Dias, P., Wofsy, S., Zhang, X., 2007. Couplings between changes in the climate system and biogeochemistry in: Solomon, S., Qin, D., Manning, M., Chen, Z., Marquis, M., Averyt, K.B., M., T., Miller, H. (Eds.), Climate Change 2007: The Physical Science Basis. Contribution of Working Group I to the Fourth Assessment Report of the Intergovernmental Panel on Climate Change. Cambridge University Press, Cambridge, United Kingdom and New York, NY, USA.

Emery, W., Meincke, J., 1986. Global water masses: summary and review. Oceanol. Acta 9, 383–391.

Etheridge, D., Steele, L., Langenfelds, R., Francey, R., Barnola, J., Morgan, V., 1996. Natural and anthropogenic changes in atmospheric CO_2 over the last 1000 years from air in Antarctic ice and firn. J. Geophys. Res. Atm. 101, 4115–4128.

Gruber, N., 1998. Anthropogenic CO_2 in the Atlantic Ocean. Global Biogeochem. Cy. 12, 165–191.

Hall, T., Plumb, R., 1994. Age as a diagnostic of stratospheric transport. J. Geophy. Res. Atm. 99, 1059–1070.

Maiss, M., Brenninkmeijer, C., 1998. Atmospheric SF_6: Trends sources and prospects. Environ. Sci. Technol. 32, 3077–3086.

Morrison, J., Codispoti, L., Smith, S., Wishner, K., Flagg, C., Gardner, W., Gaurin, S., Naqvi, S., Manghnani, V., Prosperie, L., 1999. The oxygen minimum zone in the Arabian Sea during 1995. Deep Sea Res Part II: Top. Stud. Oceanogr. 46, 1903–1931.

NOAA/ESRL, 2011. Halocarbons & other Atmospheric Trace Species Group (HATS). 〈http://www.esrl.noaa.gov/gmd/hats/index.html〉.

Oudot, C., Ternon, J., Andrie, C., Braga, E., Morin, P., 1999. On the crossing of the equator by intermediate water masses in the western Atlantic Ocean: identification and pathways of Antarctic intermediate water and upper circumpolar water. J. Geophy. Res. Oceans 104, 20911–20926.

Pierrot, D., Brown, P., Van Heuven, S., Tanhua, T., Schuster, U., Wanninkhof, R., Key, R.M., 2010. Carina tco_2 data in the atlantic ocean. Earth Syst. Sci. Data 2, 177–187.

Rhein, M., Stramma, L., 2005. Seasonal variability in the deep western boundary current around the eastern tip of Brazil. Deep-Sea Res. Part I Oceanogr. Res. Papers 52, 1414–1428.

Rhein, M., Stramma, L., Send, U., 1995. The Atlantic deep western boundary current—water masses and transports near the equator. J. Geophy. Res. Oceans. 100, 2441–2457.

Sabine, C., Feely, R., Gruber, N., Key, R., Lee, K., Bullister, J., Wanninkhof, R., Wong, C., Wallace, D., Tilbrook, B., Millero, F., Peng, T., Kozyr, A., Ono, T., Rios, A., 2004. The oceanic sink for anthropogenic CO_2. Science 305, 367–371.

Sabine, C., Tanhua, T., 2010. Estimation of anthropogenic CO_2 inventories in the ocean. Annu. Rev. Mar. Sci. 2, 175–198.

Schott, F., Junior McCreary, J., Johnson, G., 2004. Shallow overturning circulations of the tropical–subtropical oceans. In: Wang, C., Xie, S.-P., Carton, J.A. (Eds.), Earth's Climate: The Ocean–Atmosphere Interaction. AGU, Washington, DC, USA. Geophysical Monograph, pp. 261–304.

Siedler, G., Zangenberg, N., Onken, R., 1992. Seasonal changes in the Tropical Atlantic circulation—observation and simulation of the Guinea Dome. J. Geophy. Res. Oceans. 97, 703–715.

Steinfeldt, R., Tanhua, T., Bullister, J.L., Key, R.M., Rhein, M., Köhler, J., 2010. Atlantic cfc data in carina. Earth System Science Data 2, 1–15.

Stramma, L., Schott, F., 1999. The mean flow field of the tropical Atlantic Ocean. Deep-Sea Res. Part II Top. Stud. Oceanogr. 46, 279–303.

Tanhua, T., Waugh, D.W., Wallace, D.W.R., 2008. Use of SF_6 to estimate anthropogenic CO_2 in the upper ocean. J. Geophy. Res. Oceans. 113.

Tans, P., 2011. Trends in Atmospheric Carbon Dioxide (NOAA/ESRL). 〈http://www.esrl.noaa.gov/gmd/ccgg/trends/〉.

Tomczak, M., Godfrey, J., 1994. Regional Oceanography: An Introduction. Elsevier.

Touratier, F., Goyet, C., 2004. Applying the new TrOCA approach to assess the distribution of anthropogenic CO_2 in the Atlantic Ocean. J. Mar. Sys. 46, 181–197.

Touratier, F., Goyet, C., Coatanoan, C., Andrie, C., 2005. Assessments of anthropogenic CO_2 distribution in the tropical Atlantic Ocean. Deep-Sea Res. Part I Oceanogr. Res. Papers 52, 2275–2284.

Velo, A., Perez, F.F., Brown, P., Tanhua, T., Schuster, U., Key, R.M., 2009. Carina alkalinity data in the atlantic ocean. Earth Sys. Sci. Data 1, 45–61.

Walker, S., Weiss, R., Salameh, P., 2000. Reconstructed histories of the annual mean atmospheric mole fractions for the halocarbons CFC-11, CFC-12, CFC-113, and carbontetrachloride. J. Geophy. Res. Oceans. 105, 14285–14296.

Wanninkhof, R., Doney, S.C., Bullister, J.L., Levine, N.M., Warner, M., Gruber, N., 2010. Detecting anthropogenic CO_2 changes in the interior Atlantic Ocean between 1989 and 2005. J. Geophy. Res. Oceans. 115.

Warner, M., Weiss, R., 1985. Solubilities of Chlorofluorocarbon-11 and Chlorofluorocarbon-12 in water and seawater. Deep-Sea Res. Part A Oceanogr. Res. Papers 32, 1485–1497.

Warner, M., Weiss, R., 1992. Chlorofluoromethanes in South-Atlantic Antarctic intermediate water. Deep-Sea Res. Part A Oceanogr. Res. Papers 39, 2053–2075.

Warren, B., 1994. Context of the suboxic layer in the Arabian Sea. J. Earth Sys. Sci. 103, 301–314 10.1007/BF02839540.

Waugh, D., Haine, T., Hall, T., 2004. Transport times and anthropogenic carbon in the subpolar North Atlantic Ocean. Deep-Sea Res. Part I Oceanogr. Res. Papers. 51, 1475–1491.

Waugh, D., Hall, T., Haine, T., 2003. Relationship among tracer ages. J. Geophy. Res. 108.

Waugh, D.W., Hall, T.M., McNeil, B.I., Key, R., Matear, R.J., 2006. Anthropogenic CO_2 in the oceans estimated using transit time distributions. Tellus Series B Chem. Phys. Meteorol. 58, 376–389.

Weiss, R.F., Bullister, J.L., Gammon, R.H., Warner, M.J., 1985. Atmospheric chlorofluoromethanes in the deep equatorial Atlantic. Nature 314, 608–610.

Weiss, R.F., Price, B.A., 1980. Nitrous oxide solubility in water and seawater. Mar. Chem. 8, 347–359.